





A Proposal to Perform High Contrast Imaging of Human Palatine Tonsil with Cross Polarized Optical Coherence Tomography

Gargi Sharma ¹, Asha Parmar ^{1,2}, Franziska Hoffmann ³, Katharina Geißler ³, Ferdinand von Eggeling ³, Orlando Guntinas-Lichius ³ and Kanwarpal Singh ^{1,2,*}

¹ Max Planck Institute for the Science of Light, Staudtstraße 2, 91058 Erlangen, Germany; gargi.sharma@mpl.mpg.de (G.S.); asha.asha@mpl.mpg.de (A.P.)

² Department of Physics, Friedrich-Alexander Universität Erlangen-Nürnberg, Staudtstraße 7, 91058 Erlangen, Germany

³ Department of Otorhinolaryngology, Jena University Hospital, Am Klinikum 1, 07747 Jena, Germany; franziska.hoffmann@med.uni-jena.de (F.H.); katharina.geissler@med.uni-jena.de (K.G.); ferdinand.von_eggeling@med.uni-jena.de (F.v.E.); orlando.guntinas@med.uni-jena.de (O.G.-L.)

* Correspondence: kanwarpal.singh@mpl.mpg.de

Abstract: The palatine tonsils provide the first line of immune defense against foreign pathogens inhaled or ingested. However, a disruption in the epithelial layer within the tonsil crypts can lead to recurrent acute tonsillitis (RAT). Current imaging techniques suffer from poor resolution and contrast and do not allow a classification of the severity of RAT. We have developed a cross-polarized optical coherence tomography system. The system can detect a change in the polarization of the light after the light-tissue interaction. We demonstrate improved resolution and contrast in tonsil imaging with the developed method. Intensity, as well as retardance images of the excised tonsil tissue, were acquired. Features such as crypt epithelium, lymphoid follicles, and dense connective tissue were observed with improved contrast. Cross polarized optical coherence tomography can be a valuable tool in the clinic to evaluate palatine tonsils as it would allow visualizing common tonsil features without the need for any external contrast agent.

Keywords: palatine tonsils; label-free imaging; tonsillitis; chronic inflammation; cross-polarized optical coherence tomography; biomedical imaging



Citation: Sharma, G.; Parmar, A.; Hoffmann, F.; Geißler, K.; von Eggeling, F.; Guntinas-Lichius, O.; Singh, K. A Proposal to Perform High Contrast Imaging of Human Palatine Tonsil with Cross Polarized Optical Coherence Tomography. *Photonics* **2022**, *9*, 259. <https://doi.org/10.3390/photonics9040259>

Received: 22 March 2022

Accepted: 12 April 2022

Published: 13 April 2022

Publisher's Note: MDPI stays neutral with regard to jurisdictional claims in published maps and institutional affiliations.



Copyright: © 2022 by the authors. Licensee MDPI, Basel, Switzerland. This article is an open access article distributed under the terms and conditions of the Creative Commons Attribution (CC BY) license (<https://creativecommons.org/licenses/by/4.0/>).

1. Introduction

Palatine tonsils are one of the three sets of tonsils and represent a secondary immune organ. These small lymphatic oval-shaped masses protrude from each side of the oropharynx. Palatine tonsils form part of the immune system and offer the first line of defense against inhaled or ingested foreign pathogens [1,2]. Immunological processes, both humoral and cellular, are initiated in the different specialized compartments of the palatine tonsils, such as the crypt epithelium, lymphoid follicles and extrafollicular region [3]. In contrast to other immune organs, mainly due to its superficial localization directly under the oropharyngeal mucosa, the tonsils can be infected themselves, mainly by viruses or bacteria. Damage to the epithelial layer can expose the underlying basement membrane to external pathogens leading to tonsillitis. Most of these viral or bacterial infections are spread through airborne droplets in the course of a common cold. Tonsillitis can also have an odontogenic origin. Pathologically changed oral and periodontal microbiome, such as in cases of periodontal disease, can also cause tonsillitis [4,5]. The disease burden is relevant and the incidence of acute tonsillitis is high with about 100 per 1000 population per year [6]. Nevertheless, the evidence for effective treatment of acute and recurrent acute tonsillitis (RAT) is low [7,8]. An important reason for this is that it is far impossible to determine the severity of the local tonsillar infection. Hence, reliable selection criteria for or against medical or surgical treatment are missing. From a clinical point of view, it is desirable to

develop imaging techniques that can image in-vivo different parts of the tonsil tissue with high contrast and high resolution allowing for disease classification.

Current imaging techniques such as magnetic resonance imaging [9,10], computed tomography [11,12], and ultrasound [13,14] offer the possibility to image and study tonsils in three dimensions in vivo. However, due to their limited resolution, these techniques cannot provide detailed tissue morphology. At the moment, higher resolution with classical imaging techniques can only be achieved ex vivo (for instance, with 9.4 T small-bore pre-clinical magnetic resonance imaging) [15]. Optical coherence tomography (OCT) is a new imaging modality that can image biological tissues at a cellular resolution up to a depth of a few millimeters. The contrast in a standard OCT system is provided by the change in the refractive index at the interfaces of the different tissue structures. However such contrast is often not sufficient many to identify different constituents of the tissue. Recently a dual-modality system combining OCT and autofluorescence [16] was presented to image tonsil tissue with high contrast. The OCT system provided three-dimensional images of the tissue whereas the autofluorescence images enhanced the contrast for the dense connective tissue. Autofluorescence images can provide enhanced contrast for collagen and elastin [17,18] in the tissue but unfortunately, such images are not depth-resolved. Multiphoton autofluorescence systems have been reported that can acquire depth-resolved autofluorescence images, but such systems require expensive femtosecond lasers and a method to scan in the depth. As OCT systems do not require any scanning along the depth, there is a push to explore methods that would increase the contrast of the OCT images. Such improvements would make OCT systems more acceptable in the clinic. Along this line, OCT systems that can detect the change in the polarization of the light as it interacts with the tissue have been proposed. There are two variants of the OCT systems, namely polarization-sensitive optical coherence tomography (PS-OCT) systems [19–21] and cross-polarized optical coherence tomography (CP-OCT) systems [22–28] which have been demonstrated. CP-OCT systems are simpler than PS-OCT systems because such systems do not require defined polarization of light to study the tissue. CP-OCT systems have been used in the past to image collagen within the esophagus [26], oral mucosa [29], and bladder [30]. Since dense connective tissue within the tonsil is made up of collagen [16], the CP-OCT technique offers a great advantage in terms of its simplicity and enhanced contrast.

In this work, we report as a first step, high contrast ex vivo imaging of common tonsil components such as the epithelium layer of the tonsillar crypts, dense connective tissue, and lymphoid follicles using a portable CP-OCT system. Our current results suggest that in the future, the CP-OCT technique can potentially be used for in-vivo diagnosis of tonsils using an endoscopic approach.

2. Materials and Methods

2.1. Tissue Preparation

The sample tissue was a human palatine tonsil, which was resected from a patient (male, four years). Tonsillotomy was performed for tonsil hyperplasia. The procedures were in accordance with the ethical standards of the Jena University Hospital (vote of the ethics committee 3972-01/14 and 2019-1307).

After tonsillotomy, the specimen was immediately snap-frozen in liquid nitrogen and stored at -80°C until OCT measurements. For data acquisition, tissue specimen was thawed, cut along the crypts to expose the crypts surface and imaged with the CP-OCT system. The tonsil tissue was placed in a petri dish and placed under the galvo-scanner. An area of $5\text{ mm} \times 5\text{ mm}$ was scanned with a B-scan rate of 40 Hz. After the imaging, the tissue was put into a 4% formalin solution and was allowed to fixate for 12 h. Specimen processing was performed with the standard protocol by using an automatic tissue processor (Leica TP1020). These formalin-fixed paraffin-embedded (FFPE) tonsillar were sectioned in an orientation corresponding to OCT imaging into $5\text{ }\mu\text{m}$ thick slices and placed on standard glass slides. For histological correlation, the sections were hematoxylin end eosin (H&E)

stained. For digitization, the slides were scanned using the NanoZoomer slide scanner (Hamamatsu, Japan) mirror.

2.2. The OCT-Imaging

The schematic of the system is shown in Figure 1. The CP-OCT system was built using a swept-source OCT engine (Axsun Technologies, North Billerica, MA, USA). The laser had a sweeping rate of 100 kHz, central wavelength of 1310 nm, scan range of 140 nm and output power of 24 mW. The light from the laser was coupled to a broadband circulator (Thorlabs, CIR-1310-50-APC, Newton, NJ, USA) and was collimated using a lens (L1). The collimated beam of light was split into two parts using a non-polarizing (50/50) beam splitter (Thorlabs, BS012, Newton, NJ, USA) NPBS1. One part of the light beam was used as the reference signal and another part of the beam was directed toward the sample. The light in the reference arm was further divided into two parts using a non-polarizing (50/50) beam splitter (Thorlabs, BS012, Newton, NJ, USA) NPBS2. The transmitted part of the reference beam after the NPBS2 was reflected using a mirror M1. This part of the reference signal had the same polarization as the signal after the lens L1. The reflected part of the beam after the NPBS2 was reflected using the mirror M2 making a double pass through an achromatic quarter-wave plate (Thorlabs, AQWP10M-1600, Newton, NJ, USA). The quarter-wave plate was oriented in a way that it changed the polarization of the light from the mirror M2, orthogonal to the light reflected from mirror M1. Combined light reflected from mirror M1 and M2 made the reference signals. In the sample arm side after the NPBS1, the light was focused using a 25 mm focal length lens L3. The intensity of the light measured on the sample was 9 mW. The light was scanned on the sample using a Galvo-scanner (Thorlabs, GVS012, Newton, NJ, USA). The light was reflected from the reference mirrors M1 and M2, and the sample was interfered at the NBPS1. The interfered signals split into two parts at the NBPS1. One part after passing through the circulator's third arm was detected using detector D1. The second part was coupled to a fiber using a lens (L2) and detected using a detector D2. The signals from the detectors D1 and D2 were fed to a balanced detector which allowed to remove the common mode noise of the system [31]. The signal from the balanced detector was digitized using a 12 bit, 500 MS/s digitizer. A Hamming window was applied over the digitized signal from the digitizer before performing Fourier transform which resulted in the axial scan of the sample. 2500 axial scans were collected together to make a B-scan of the sample and transferred to the host computer as JPEG images. A LabVIEW-based software was developed to collect the images from the OCT engine and save them to the computer disk.

The two reference signals from the mirrors M1 and M2 were delayed with respect to each other to produce depth encoded, co-polarized and cross-polarized images of the sample. For calculation of the contrast between different sections of the images, we calculated Michelson contrast defined as

$$Contrast = \frac{|I_{avg}(A) - I_{avg}(B)|}{I_{avg}(A) + I_{avg}(B)} \quad (1)$$

where $I_{avg}(A)$ and $I_{avg}(B)$ are the average intensities in section A and section B of the image.

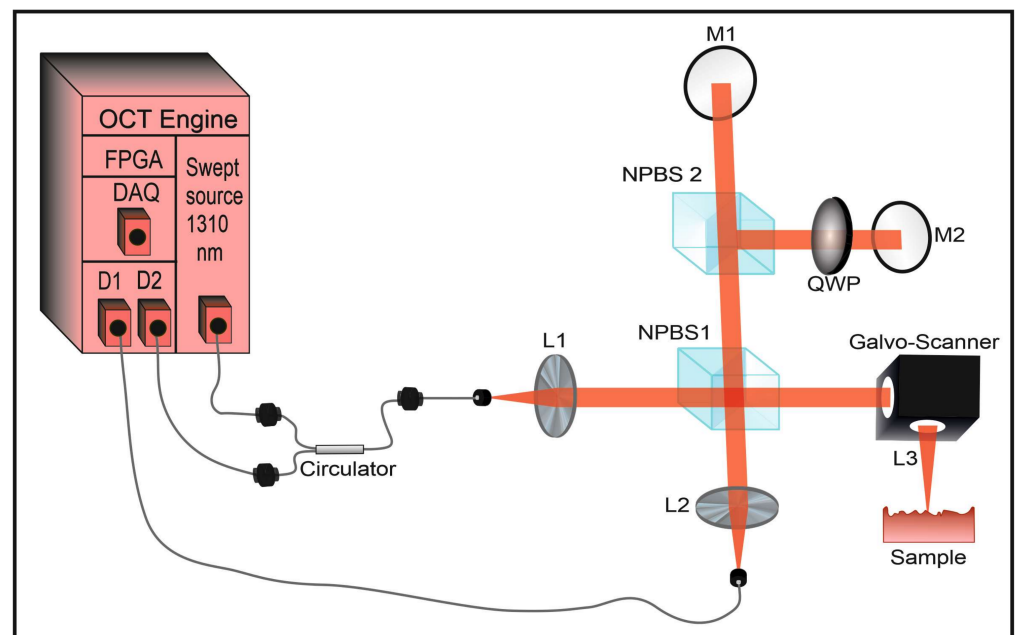


Figure 1. Schematic of the cross-polarized optical coherence tomography system. The abbreviated components of the system are optical coherence tomography (OCT), field-programmable gate array (FPGA), data acquisition card (DAQ), diode (D), lens (L), non-polarizing beam splitter (NPBS), quarter-wave plate (QWP), mirror (M).

3. Results

The system was characterized for its axial resolution, lateral resolution, and sensitivity of 5.1 μm , 13 μm , and 105 dB respectively. A representative B-Scan of the tonsil is shown in Figure 2. In the top panel Figure 2a, the cross-sectional cross-polarized image of the tonsil is shown. In Figure 2b, the co-polarized image of the tonsil at the same location is shown. It can be seen from Figure 2 that the dense connective tissue (DCT) is seen with high contrast in the cross-polarized image compared to the co-polarized image. Other features such as the epithelial layer of the tonsillar crypts and lymphoid follicles (LF) can also be seen in these images. The epithelial layer was found to be approximately 180 μm . The contrast between DCT and Epithelial layer calculate using Equation 1 was found to be 0.14 and 0.37 for co-polarized and cross-polarized images respectively. This suggests an approximately 3-fold increase in the contrast between DCT and Epithelial layer when imaged with crossed-polarized OCT. Similarly, an approximately a two-fold contrast increase was observed between DCT and lymphoid follicles when imaged with crossed-polarized OCT.

Furthermore, en face images of the tonsil were acquired by cutting the tonsil tissue at two different locations. In Figure 3 top row, images just below the top surface of the tonsil are shown whereas in the bottom row, the images of the tonsil cut approximately 5 mm below the top surface are shown. In Figure 3a, H&E-stained image of the tonsil is shown. Areas with DCT and LF can be seen in the H&E-stained image. In Figure 3b, an en face image generated from the co-polarized image of the tonsil is shown. It can be seen that the DCT shows up poorly in the intensity image. In Figure 3c, the cross-polarized image of the tonsil tissue is shown and one can immediately appreciate the enhanced contrast of the DCT in the cross-polarized image. A similar improvement in the DCT contrast is seen in the images of the tissue cut 5 mm below the crypt surface of the tonsil.

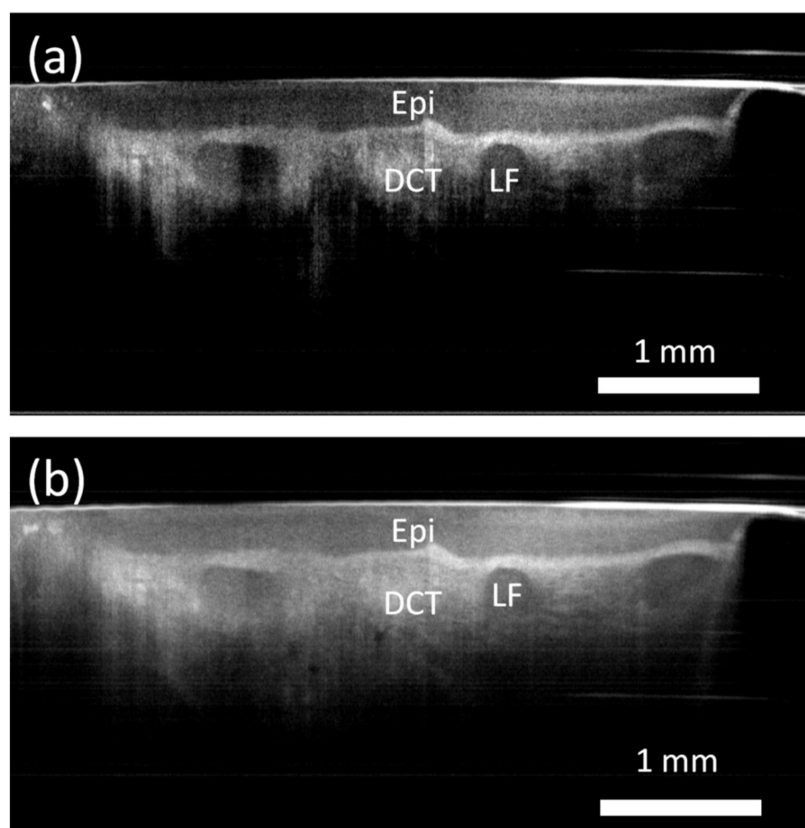


Figure 2. (a) Cross-sectional cross-polarized image of the tonsil tissue. (b) Cross-sectional co-polarized image of tonsil tissue at the same location as the top image. Different features such as the reticulated crypt epithelium (Epi), dense connective tissue (DCT), and lymphoid follicles (LF) can be visualized.

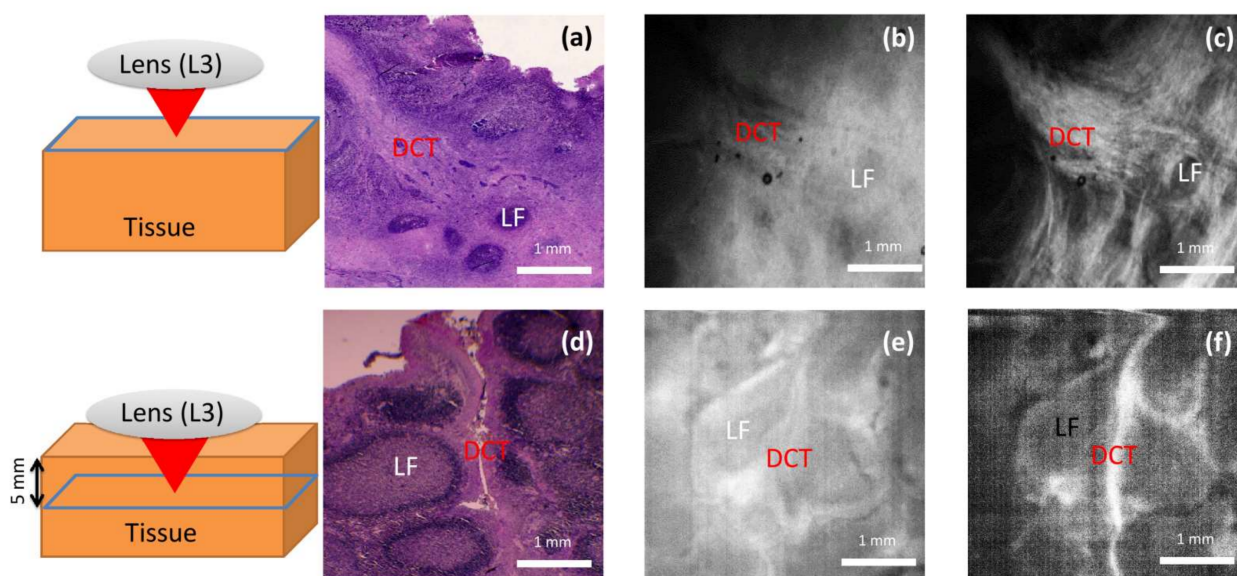


Figure 3. En face images of the tonsil acquired near the top surface of the tonsil are shown in the top row and the images acquired 5 mm below the top surface are shown in the bottom row. H&E stained image of the tonsil (a,d), co-polarized image of the tonsil (b,e), and cross-polarized image of the tonsil (c,f). Different features such as the dense connective tissue (DCT) and lymphoid follicles (LF) can be visualized.

4. Discussion

Our results suggest that a two to three-fold increase in the contrast between different tonsil features can be obtained using cross-polarized OCT which demonstrates the merits of cross-polarized OCT imaging over standard co-polarized OCT imaging. Previously [16], a combination of autofluorescence and OCT has been used to increase the contrast in tonsil tissue. A combination of two systems increases the complexity and still does not provide subsurface images since the autofluorescence is limited to the top surface only. Compared to magnetic resonance imaging [9,10], computed tomography [11,12], and ultrasound [13,14], our technique offers better resolution without any contrast agent. However, our technique in its current form also has some drawbacks. The current system is suitable for ex-vivo imaging only and not for in-vivo imaging. Furthermore, the developed system does not provide cellular resolution. In the future, this technique can be combined with high-resolution OCT systems to achieve cellular resolution and improved contrast. Endoscopic implementation [32,33] of the same would allow imaging epithelial layer morphology within the crypts which would increase the clinical value of the technique in diseases such as tonsillar cancer and recurrent tonsillitis.

5. Conclusions

We have tested the feasibility of using CP-OCT to improve the contrast of various features of the tonsil tissue. To our knowledge, this is the first time wherein improved contrast in tonsil imaging with cross-polarized optical coherence tomography has been demonstrated. The ability of this technique to provide high-resolution images of the tonsil tissue without the use of any external contrast agent holds great promise in the clinic to diagnose tonsil tissue. Although the imaging depth is limited to only a few millimeters into the tissue, in the future, this can be circumvented with the use of flexible optical fiber probes.

Author Contributions: Conceptualization, F.v.E., O.G.-L. and K.S.; methodology, G.S., A.P., F.H., K.G., F.v.E. and K.S.; writing—original draft preparation, G.S., F.v.E. and K.S.; writing—review and editing, F.v.E., O.G.-L., F.H. and K.S.; supervision, F.v.E., O.G.-L. and K.S. All authors have read and agreed to the published version of the manuscript.

Funding: This work was supported by the Max Planck Society for the Advancement of Science. CRIMSON—Coherent Raman Imaging for the molecular study of the origin of diseases (EU Horizon 2020-ICT; 101016923).

Institutional Review Board Statement: The procedures were in accordance with the ethical standards of the Jena University Hospital.

Informed Consent Statement: Informed consent was obtained from all subjects involved in the study.

Data Availability Statement: Data underlying the results presented in this paper are available upon request.

Conflicts of Interest: The authors declare no conflict of interest.

References

1. Carrasco, A.; Sjölander, I.; Van Acker, A.; Dernstedt, A.; Fehrm, J.; Forsell, M.; Friberg, D.; Mjösberg, J.; Rao, A. The Tonsil Lymphocyte Landscape in Pediatric Tonsil Hyperplasia and Obstructive Sleep Apnea. *Front. Immunol.* **2021**, *12*, 674080. [[CrossRef](#)] [[PubMed](#)]
2. Scadding, G.K. Immunology of the tonsil: A review. *J. R. Soc. Med.* **1990**, *83*, 104–107. [[CrossRef](#)] [[PubMed](#)]
3. Nave, H.; Gebert, A.; Pabst, R. Morphology and immunology of the human palatine tonsil. *Anat. Embryol.* **2001**, *204*, 367–373. [[CrossRef](#)] [[PubMed](#)]
4. Georgalas, C.; Kanagalingam, J.; Zainal, A.; Ahmed, H.; Singh, A.; Patel, K.S. The association between periodontal disease and peritonsillar infection: A prospective study. *Otolaryngol. Head Neck Surg.* **2002**, *126*, 91–94. [[CrossRef](#)]
5. Barone, A.; Chatelain, S.; Derchi, G.; Di Spirito, F.; Martuscelli, R.; Porzio, M.; Sbordone, L. Antibiotic's effectiveness after erupted tooth extractions: A retrospective study. *Oral Dis.* **2020**, *26*, 967–973. [[CrossRef](#)] [[PubMed](#)]
6. Georgalas, C.C.; Tolley, N.S.; Narula, P.A. Tonsillitis. *BMJ Clin. Evid.* **2014**, *22*, 0503.
7. Burton, M.J.; Glasziou, P.P.; Chong, L.Y.; Venekamp, R.P. Tonsillectomy or adenotonsillectomy versus non-surgical treatment for chronic/recurrent acute tonsillitis. *Cochrane Database Syst. Rev.* **2014**, *2014*, CD001802. [[CrossRef](#)]

8. Munck, H.; Jørgensen, A.W.; Klug, T.E. Antibiotics for recurrent acute pharyngo-tonsillitis: Systematic review. *Eur. J. Clin. Microbiol. Infect. Dis.* **2018**, *37*, 1221–1230. [\[CrossRef\]](#)
9. Çelebi, İ.; Bozkurt, G.; Polat, N. Tonsillar Plasmacytoma: Clues on magnetic resonance imaging. *BMC Med. Imaging* **2018**, *18*, 19. [\[CrossRef\]](#)
10. El Sherif, I.; Shembesh, F.M. A tonsillolith seen on MRI. *Comput. Med. Imaging Graph.* **1997**, *21*, 205–208. [\[CrossRef\]](#)
11. Aspestrand, F.; Kolbenstvedt, A.; Boysen, M. Staging of carcinoma of the palatine tonsils by computed tomography. *J. Comput. Assist. Tomogr.* **1988**, *12*, 434–437. [\[CrossRef\]](#) [\[PubMed\]](#)
12. Oda, M.; Kito, S.; Tanaka, T.; Nishida, I.; Awano, S.; Fujita, Y.; Saeki, K.; Matsumoto-Takeda, S.; Wakasugi-Sato, N.; Habu, M.; et al. Prevalence and imaging characteristics of detectable tonsilloliths on 482 pairs of consecutive CT and panoramic radiographs. *BMC Oral Health* **2013**, *13*, 54. [\[CrossRef\]](#) [\[PubMed\]](#)
13. Kay-Rivest, E.; Saint-Martin, C.; Daniel, S.J. High-frequency ultrasound: A novel diagnostic tool to measure pediatric tonsils in 3 dimensions. *Otolaryngol. Head Neck Surg.* **2019**, *161*, 856–861. [\[CrossRef\]](#) [\[PubMed\]](#)
14. Hosokawa, T.; Yamada, Y.; Tanami, Y.; Hattori, S.; Sato, Y.; Hosokawa, M.; Oguma, E. Evaluation of the normal tonsils in pediatric patients with ultrasonography. *J. Ultrasound Med.* **2017**, *36*, 1029–1036. [\[CrossRef\]](#)
15. Herrmann, K.H.; Hoffmann, F.; Ernst, G.; Pertzborn, D.; Pelzel, D.; Geißler, K.; Guntinas-Lichius, O.; Reichenbach, J.R.; von Eggeling, F. High-resolution MRI of the human palatine tonsil and its schematic anatomic 3D reconstruction. *J. Anat.* **2022**, *240*, 166–171. [\[CrossRef\]](#)
16. Pahlevaninezhad, H.; Lee, A.M.; Rosin, M.; Sun, I.; Zhang, L.; Hakimi, M.; MacAulay, C.; Lane, P.M. Optical coherence tomography and autofluorescence imaging of human tonsil. *PLoS ONE* **2014**, *9*, e115889. [\[CrossRef\]](#)
17. Monici, M. Cell and tissue autofluorescence research and diagnostic applications. *Biotechnol. Annu. Rev.* **2005**, *11*, 227–256. [\[CrossRef\]](#)
18. Banerjee, B.; Miedema, B.E.; Chandrasekhar, H.R. Role of basement membrane collagen and elastin in the autofluorescence spectra of the colon. *J. Invest. Med.* **1999**, *47*, 326–332.
19. Sharma, S.; Hartl, G.; Naveed, S.K.; Blessing, K.; Sharma, G.; Singh, K. Input polarization-independent polarization-sensitive optical coherence tomography using a depolarizer. *Rev. Sci. Instrum.* **2020**, *91*, 043706. [\[CrossRef\]](#)
20. De Boer, J.F.; Hitzenberger, C.K.; Yasuno, Y. Polarization sensitive optical coherence tomography—A review [Invited]. *Biomed. Opt. Express* **2017**, *8*, 1838–1873. [\[CrossRef\]](#)
21. Wang, Z.; Lee, H.-C.; Ahsen, O.O.; Lee, B.; Choi, W.; Potsaid, B.; Liu, J.; Jayaraman, V.; Cable, A.; Kraus, M.F. Depth-encoded all-fiber swept source polarization sensitive OCT. *Biomed. Opt. Express* **2014**, *5*, 2931–2949. [\[CrossRef\]](#) [\[PubMed\]](#)
22. Schmitt, J.; Xiang, S. Cross-polarized backscatter in optical coherence tomography of biological tissue. *Opt. Lett.* **1998**, *23*, 1060–1062. [\[CrossRef\]](#) [\[PubMed\]](#)
23. Sharma, G.; Sharma, S.; Blessing, K.; Hartl, G.; Waldner, M.; Singh, K. Swept source cross-polarized optical coherence tomography for any input polarized light. *J. Opt.* **2020**, *22*, 045301. [\[CrossRef\]](#)
24. Hartl, G.R.; Parmar, A.; Sharma, G.; Singh, K. Cross-Polarized Optical Coherence Tomography System with Unpolarized Light. *Photonics* **2022**, *9*, 76. [\[CrossRef\]](#)
25. Gelikonov, V.; Gelikonov, G. New approach to cross-polarized optical coherence tomography based on orthogonal arbitrarily polarized modes. *Laser Phys. Lett.* **2006**, *3*, 445. [\[CrossRef\]](#)
26. Kuranov, R.V.; Sapozhnikova, V.; Turchin, I.; Zagaynova, E.; Gelikonov, V.; Kamensky, V.; Snopova, L.; Prodanetz, N. Complementary use of cross-polarization and standard OCT for differential diagnosis of pathological tissues. *Opt. Express* **2002**, *10*, 707–713. [\[CrossRef\]](#)
27. Yao, X.; Gan, Y.; Ling, Y.; Marboe, C.C.; Hendon, C.P. Multicontrast endomyocardial imaging by single-channel high-resolution cross-polarization optical coherence tomography. *J. Biophotonics* **2018**, *11*, e201700204. [\[CrossRef\]](#)
28. Alghilan, M.A.; Lippert, F.; Platt, J.A.; Eckert, G.J.; González-Cabezas, C.; Fried, D.; Hara, A.T. In vitro longitudinal evaluation of enamel wear by cross-polarization optical coherence tomography. *Dent. Mater.* **2019**, *35*, 1464–1470. [\[CrossRef\]](#)
29. Gladkova, N.; Kiseleva, E.; Robakidze, N.; Balalaeva, I.; Karabut, M.; Gubarkova, E.; Feldchtein, F. Evaluation of oral mucosa collagen condition with cross-polarization optical coherence tomography. *J. Biophotonics* **2013**, *6*, 321–329. [\[CrossRef\]](#)
30. Gladkova, N.; Streltsova, O.; Zagaynova, E.; Kiseleva, E.; Gelikonov, V.; Gelikonov, G.; Karabut, M.; Yunusova, K.; Evdokimova, O. Cross-polarization optical coherence tomography for early bladder-cancer detection: Statistical study. *J. Biophotonics* **2011**, *4*, 519–532. [\[CrossRef\]](#)
31. Podoleanu, A.G. Unbalanced versus balanced operation in an optical coherence tomography system. *Appl. Opt.* **2000**, *39*, 173–182. [\[CrossRef\]](#) [\[PubMed\]](#)
32. Blessing, K.; Schirmer, J.; Parmar, A.; Singh, K. Depth encoded input polarisation independent swept source cross-polarised optical coherence tomography probe. *J. Phys. D Appl. Phys.* **2021**, *54*, 305401. [\[CrossRef\]](#)
33. Blessing, K.; Schirmer, J.; Sharma, G.; Singh, K. Novel input polarisation independent endoscopic cross-polarised optical coherence tomography probe. *J. Biophotonics* **2020**, *13*, e202000134. [\[CrossRef\]](#) [\[PubMed\]](#)